JACS
JOURNAL OF THE AMERICAN CHEMICAL SOCIETY
Communication
pubs.acs.org/JACS

Self-Illuminating ^{64}Cu-Doped CdSe/ZnS Nanocrystals for in Vivo Tumor Imaging

Xiaolian Sun,[†,§] Xinglu Huang,[†,§] Jinxia Guo,[†,‡] Wenlei Zhu,[§] Yong Ding,[∥] Gang Niu,[†] Andrew Wang,[⊥] Dale O. Kiesewetter,[†] Zhong Lin Wang,[∥] Shouheng Sun,[§] and Xiaoyuan Chen*[,†]

[†]Laboratory of Molecular Imaging and Nanomedicine, National Institute of Biomedical Imaging and Bioengineering, National Institutes of Health, Bethesda, Maryland 20892, United States

[‡]Center for Molecular Imaging and Translational Medicine, School of Public Health, Xiamen University, Xiamen, Fujian 361102, China

[§]Department of Chemistry, Brown University, Providence, Rhode Island 02912, United States

[∥]School of Materials Science and Engineering, Georgia Institute of Technology, Atlanta, Georgia 30332, United States

[⊥]Ocean NanoTech LLC, Springdale, Arkansas 72764, United States

Supporting Information

ABSTRACT: Construction of self-illuminating semiconducting nanocrystals, also called quantum dots (QDs), has attracted much attention recently due to their potential as highly sensitive optical probes for biological imaging applications. Here we prepared a self-illuminating QD system by doping positron-emitting radionuclide ^{64}Cu into CdSe/ZnS core/shell QDs via a cation-exchange reaction. The ^{64}Cu-doped CdSe/ZnS QDs exhibit efficient Cerenkov resonance energy transfer (CRET). The signal of ^{64}Cu can accurately reflect the biodistribution of the QDs during circulation with no dissociation of ^{64}Cu from the nanoparticles. We also explored this system for in vivo tumor imaging. This nanoprobe showed high tumor-targeting ability in a U87MG glioblastoma xenograft model (12.7% ID/g at 17 h time point) and feasibility for in vivo luminescence imaging of tumor in the absence of excitation light. The availability of these self-illuminating integrated QDs provides an accurate and convenient tool for in vivo tumor imaging and detection.

Optical imaging is a powerful technique with many advantages such as high sensitivity, low-cost, and short acquisition time.[1−3] Various inorganic nanomaterials[4−12] (e.g., carbon dots,[4,5] upconversion nanoparticles,[6,7] and quantum dots[8−12]) have been explored as fluorescent probes for biological imaging. Among these, quantum dots (QDs) attract much attention due to their unique optical properties such as size- and composition-dependent fluorescence emission wavelength, high quantum yield, and high photostability.[8−12] However, the use of existing quantum dots requires the excitation from external illumination sources, and this is challenging for in vivo imaging because of the strong autofluorescence background arising from ubiquitously expressed endogenous chromophores as well as the light-absorption and -scattering properties of biological tissue.[13] QD-based energy transfer systems, primarily consisting of bioluminescence resonance energy transfer (BRET), chemiluminescence resonance energy transfer (CLRET), and Cerenkov resonance energy transfer (CRET) systems, in which QDs serve as energy acceptors in the presence of an internal instead of an external light source, have attracted much attention due to their low background and high detection sensitivity.[14−17] So et al. designed luciferase conjugated QDs based on the principle of BRET. Upon the addition of renilla luciferase (rLuc) substrate coelenterazine, the bioluminescence energy of the luciferase-catalyzed reaction occurs and transfers to the QDs to emit. The in vivo signal-to-background ratio of this self-illuminating QD conjugate appears to be higher than that of QDs excited by external light.[14] In Zhang's CLRET system, a mixture of luminol and QDs was administered to mice to detect myeloperoxidase (MPO) activity. The chemiluminescence generated by the luminol and MPO-excited QDs can penetrate through tissues, resulting in a much higher in vivo signal than using luminol only.[15]

In recent years, the CRET system, which bridges radionuclide imaging with optical imaging, has attracted more attention. Cerenkov luminescence (CL) is produced when charged particles (β- or α-particles) travel through a dielectric medium, such as water, with a velocity that exceeds the speed of light in that medium.[18,19] CL is expected to have a low autofluorescence background since no excitation light is required. CL spectra are continuous, being more intense at higher frequencies (ultraviolet/blue).[20] Since the ultraviolet/blue wavelengths are highly attenuated by tissues, CL itself is not suitable for in vivo imaging. In the QD-CRET system, the CL energy transferred to the QDs in close proximity can help convert the blue-weighted CL to longer QDs emission wavelengths which allows for optical imaging in live animals.[21,22] However, up to now, most QD-CRET systems were still based on the random interactions between the CL source and QDs in solution,[21] which could result in a mismatch between the biodistribution of the CL source and that of the QDs. Here, for the first time, we report the design of a QD-CRET system with the CL source doped inside the QDs in a controllable way.

Received: October 10, 2013
Published: January 8, 2014

   dx.doi.org/10.1021/ja410438n | J. Am. Chem. Soc. 2014, 136, 1706−1709

Our designed, self-illuminating QDs are prepared by directly doping ^{64}Cu [$t_{1/2}$ = 12.7 h; β^+, 0.653 MeV (17.8%); β^-, 0.579 MeV (38.4%)] into various QDs via a cation-exchange reaction. The decay characteristics of ^{64}Cu allow for CRET.[19] First, the close interaction between ^{64}Cu and QDs in this design leads to a significant enhancement in CRET efficiency compared with the previous method of randomly mixing ^{64}Cu and QDs together. Second, our ^{64}Cu-doped QDs are stable under physiological conditions with no detachment of ^{64}Cu from QDs during circulation. The detachment of ^{64}Cu can cause a mismatch between the localization of ^{64}Cu and that of QDs, which is a major concern for the in vivo application of ^{64}Cu-labeled QD system. Even when ^{64}Cu ions are attached to QDs via metal chelators, detachment can still happen due to the transchelation of radiometal from the chelate or by the dissociation of the radionuclide-containing polymer coating from the nanoparticle in the presence of high salt and protein concentrations.[23] For our ^{64}Cu-doped QDs, the signal of radionuclide can accurately reflect the localization of the QDs. Finally, these ^{64}Cu-doped QDs have a "clear" surface without the need to conjugate additional energy donors. It is well-known that the biodistribution properties of nanoparticles are highly dependent on their surface properties.[24] After being stabilized with polyethylene glycol (PEG), these chelator-free ^{64}Cu-doped QDs have been successfully used for luminescence and positron emission tomography (PET) imaging in a xenograft tumor model with high tumor-to-background contrast.

Cu can be encapsulated into ionic QDs via a place exchange between Cu^+ and the original cation.[25−27] After this reaction, the size and shape of the original ionic nanostructure is conserved, while the composition has been altered. This reaction has been widely used to tune the fluorescence properties of QDs. Here we used the cation-exchange reaction to dope a trace amount of ^{64}Cu radioisotope into QDs, therefore rendering the QDs with new luminescence properties (Figure 1). To demonstrate this strategy, three different kinds

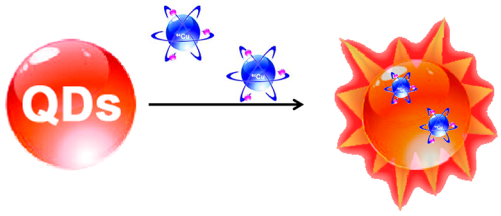

Figure 1. Design of self-illuminating ^{64}Cu-doped QDs.

of organic-soluble CdSe/ZnS core/shell QDs with emission wavelengths around 526, 580, and 636 nm (QD526, QD580, and QD636) were chosen as model compounds. We first began the reaction with nonradioactive $CuCl_2$ to evaluate the feasibility of doping Cu^{2+} into CdSe/ZnS QDs. In a typical reaction between QD636 and $CuCl_2$, QD636 were dispersed in a mixture of hexane and ethanol in the presence of ascorbic acid, different amounts of $CuCl_2$ (Cu:Se = 1:20, 1:2, and 20:1) were added dropwise respectively, and the solution was slowly heated to 60 °C and kept at that temperature for 1 h to ensure the completion of the reaction. After purification, the product was dispersed in ethanol. The composition of $CuCl_2$-treated QDs was analyzed by inductively coupled plasma-atomic emission spectroscopy (ICP-AES) (Table S1, Supporting Information [SI]) and X-ray energy-dispersive spectroscopy (EDS) (Figure S2, SI), which showed a decrease of Zn-to-Se (anion ion) ratio first and a decrease of both Zn-to-Se and Cd-to-Se ratios as the Cu-to-Se ratio gradually increased, indicating that Cu could replace Zn, and even diffuse inside the core to replace Cd under this reaction condition. This was further confirmed by the high-angle, annular dark-field scanning TEM (HAADF-STEM) images. Although the size and morphology of QD were well maintained after this cation-exchange reaction (Figure S1A,B, SI), the high resolution line-scan EDS analysis across a single QD showed Cu distributed throughout the QD with the shell containing more (Figure S1C−F, SI). UV and fluorescence properties also changed as the composition changed (Figure S3, SI). All the observations proved that the Cu^{2+} ions replaced the existing cations and were doped inside QDs under this reaction condition. The integration of ^{64}Cu into QDs was performed by following the same procedure for preparing nonradioactive Cu-doped QDs except that $^{64}CuCl_2$ solution was used instead of $CuCl_2$. The ^{64}Cu-labeling yield was nearly 100% for all three QDs as determined by γ counting, indicating that the labeling method is very robust and generally applicable. The specific activity of the radiolabeled QDs is tunable by varying the concentration of the $^{64}CuCl_2$ precursor in this reaction. Considering that the amount of $^{64}CuCl_2$ (200 μCi/mg QDs) used here is below the detection limit of ICP (~ng/mL), and that ^{64}Cu decays into ^{64}Ni and ^{64}Zn, no obvious changes in morphology or UV and fluorescence properties were observed in all three QDs after ^{64}Cu doping (Figure S4−6, SI). The ^{64}Cu-doped QDs were further made water-soluble by modification with amine-polyethylene glycol-(PEG)-thiol (MW = 5000). It is worth noting that for water-soluble QDs which were already coated with polymers, the ^{64}Cu-labeling efficiency was less than 10% under the same conditions. This further proved that ^{64}Cu ions diffused into QDs instead of physically adsorbing onto QDs and this diffusion could be blocked by large-molecular-weight polymers. Once ^{64}Cu is doped inside QDs, the interaction between ^{64}Cu and QDs is very strong with negligible release of ^{64}Cu after incubation in fetal bovine serum and mouse blood at 37 °C for 48 h (Figure S7, SI). The amine-PEG_{5000}-thiol-coated QDs have hydrodynamic sizes of 14.1 ± 1.1 (QD526), 18.5 ± 0.9 (QD580), and 28.4 ± 2.1 nm (QD636) (Table S2, SI) with no aggregation and are thus suitable for in vivo study.

We first investigated the in vitro Cerenkov luminescence from ^{64}Cu-doped QDs using a conventional small-animal in vivo imaging system (IVIS) Lumina optical imaging system. As a first demonstration, the radiance of $^{64}CuCl_2$ aqueous solution under different filters was collected (Figure S8, SI). A plot of the photon flux extracted from the phantom versus the filter wavelength is shown in Figure 2C. The $^{64}CuCl_2$ displayed a continuous luminescence spectrum with wavelengths below 500 nm being more intense, consistent with reference reports.[20] The total photon flux was linearly correlated with the amount of $^{64}CuCl_2$ radioactivity both in the absence (Figure S9, SI) and in the presence (Figure S10A,B, SI) of QDs, which was also related to the amount of QDs added (Figure S10C,D, SI). In the following phantom study we thus fixed the amount of ^{64}Cu at 46 μCi and the amount of QDs at 10 μg for all the samples as a demonstration. Figure 2A summarized the phantom results of ^{64}Cu-doped QDs, mixture of ^{64}Cu and QDs, free ^{64}Cu as well as QDs. PET images confirmed that all the samples were well-dispersed with the same signal intensity. The total photon flux extracted from the luminescence phantom was summarized in Figure 2B. QDs alone without excitation light did not produce

dx.doi.org/10.1021/ja410438n | J. Am. Chem. Soc. 2014, 136, 1706−1709

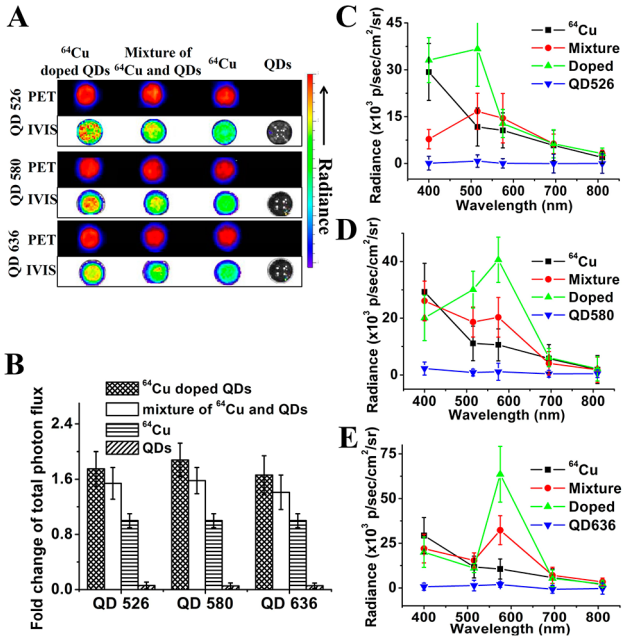

Figure 2. (A) PET and optical images of aqueous suspensions of QDs (nonradioactive), free $^{64}CuCl_2$, mixture of $^{64}CuCl_2$ and QDs, and ^{64}Cu-doped QDs with the same amount of ^{64}Cu radioactivity. (B) Comparison of the total photon flux extracted from the phantom images in (A). QDs without excitation light and ^{64}Cu presence had virtually no photoluminescence. The total photon flux recorded from the IVIS system without emission filter followed the order of ^{64}Cu-doped QDs > ^{64}Cu mixed with QDs > ^{64}Cu. (C–E) Photon flux obtained from ^{64}Cu, mixture of ^{64}Cu and QDs, ^{64}Cu-doped QDs as well as QDs with QD526 (C), QD580 (D), and QD636 (E) under different emission filters versus the filter wavelengths. Increased photon flux at the emission wavelength of the QDs reflects effective Cerenkov resonance energy transfer (CRET).

luminescence. Compared with free ^{64}Cu, we noted a 1.5-fold enhancement on total photon flux when ^{64}Cu was mixed with QDs and 1.75-fold enhancement when ^{64}Cu was doped into QDs. With the knowledge that the IVIS spectrum we used here can only cover wavelengths ranging from 400 to 920 nm, a reasonable explanation for this phenomenon is that the presence of QDs helps to convert photons within the ultraviolet range that are undetectable by the IVIS system into photons with longer wavelengths (via CRET effect) which can be captured by the system. Take QD520 as an example, as shown in Figure 2C, the addition of QD520 red-shifted the light intensity peak from 400 to 515 nm which is close to the emission wavelength of QD520. In addition, in the presence of the same amount of radioactivity and QDs, ^{64}Cu-doped QD520 had twice as much light intensity around 515 nm than that of the mixture of ^{64}Cu and QD520, indicating that doping ^{64}Cu inside the QDs can greatly improve the energy transfer efficiency. The samples with QD580 (Figure 2D) and QD636 (Figure 2E) shared the same trend with the luminescence intensity peak further red-shifted to their respective emission wavelengths. Another factor that could contribute to the enhancement of luminescence by doping ^{64}Cu into different QDs is the refractive index, as Cerenkov luminescence is refractive index dependent.[28] QD could provide a medium with higher refractive index for charged particles than water or biological fluid. Thus, more luminescence light can be produced by ^{64}Cu-doped QDs than ^{64}Cu in water and mixture of ^{64}Cu and QDs.

Next we explored the *in vivo* biodistribution of ^{64}Cu-doped QDs in a U87MG glioblastoma xenograft model by PET. In a typical study, tumor mice were IV-injected with 25 μg QD580 (250 μCi ^{64}Cu). Here, we chose QD580 as a compromise between the predicted tumor-targeting ability and luminescence imaging ability; it is expected that smaller QDs (with shorter emission wavelength) may exhibit higher in vivo passive targeting efficacy based on enhanced permeability and retention (EPR) effect,[29] while longer wavelength emission light is preferred for optical imaging. In the whole-body PET imaging of mice, liver, spleen and tumor were all clearly visualized (Figure 3A). Quantitative region-of-interest (ROI) analysis of

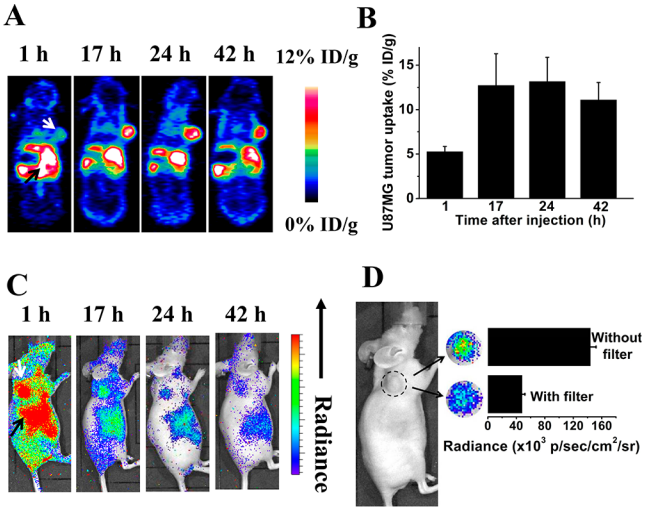

Figure 3. (A) Representative whole-body coronal PET images of U87MG tumor-bearing mice at 1, 17, 24, and 42 h after intravenous injection of 250 μCi of ^{64}Cu-doped QD580 (n = 3). White arrow, tumor area; black arrow, liver area. Slices for the images are 1 mm thick. QDs show typical reticuloendoethlial system uptake in the liver and spleen as well as tumor accumulation via an EPR effect. (B) ROI analysis of U87MG tumor uptake of ^{64}Cu-doped QDs over time (n = 3). (C) Representative whole-body luminescence images of U87MG tumor-bearing mice at 1, 17, 24, and 42 h postinjection of 250 μCi of ^{64}Cu-doped QD580 (n = 3). White arrow, tumor area; black arrow, liver area. (D) Comparison of photon flux obtained via an open window without filter and that obtained via a filter covered from 575 to 650 nm in the tumor area 42 h postinjection of 250 μCi of ^{64}Cu-doped QDs.

the whole-body PET images showed about 5% ID/g uptake of ^{64}Cu-doped QDs in the U87MG tumor at the 1 h time point, which reached 12.7% ID/g at 17 h and still retained over 10% ID/g even at the 42-h time point. The high tumor uptake suggests potential use of these QDs for cancer imaging. A major concern here is whether the PET imaging could truly reflect the distribution of QDs. Since PET imaging detects the radiolabel rather than the nanoparticles directly, the detachment of radionuclide from the nanoparticles could lead to inaccurate description of the pharmacokinetics of the nanoparticles. We thus sacrificed the mice after the in vivo PET imaging study at 45 h postinjection of ^{64}Cu-doped QDs. The ex vivo PET imaging of tissues of interest is shown in Figure S11A, SI. The trend of signal intensity is similar to that of in vivo PET imaging (Figure S12, SI). Analysis of ^{64}Cu radioactivity via γ counting found that the heart-, liver-, tumor-, spleen-, lung-, and kidney-

dx.doi.org/10.1021/ja410438n | J. Am. Chem. Soc. 2014, 136, 1706–1709

to-muscle ratios were around 3.9 ± 2.1, 11.7 ± 7.2, 5.2 ± 1.3, 23.1 ± 10.6, 4.8 ± 0.7, 4.3 ± 1.3, respectively (Table S3, SI). ICP measurement was also carried out to quantify the QD amount in the tissue homogenate. The heart-, liver-, tumor-, spleen-, lung-, kidney-to-muscle ratio based on ICP were around 1.9 ± 0.2, 8.4 ± 3.5, 5.2 ± 0.7, 19.2 ± 5.7, 2.0 ± 0.4, 1.2 ± 0.3, respectively (Figure S3, SI). The results obtained by ICP were linearly correlated with the PET imaging results (Figure S11B, SI). Thus, PET imaging in this study could truly reflect the biodistribution of ^{64}Cu-doped QDs. Compared with previous studies based on ^{64}Cu-chelated QDs,[30] our ^{64}Cu-doped QDs have a relatively high tumor-targeting efficacy which is very important for cancer imaging.

Next we evaluated using ^{64}Cu-doped QD580 for in vivo luminescence imaging in the absence of excitation light. Similarly, 25 μg QDs (250 μCi ^{64}Cu) was injected intravenously to U87MG tumor mice via tail vein, and luminescence images were sequentially captured using IVIS. Time-dependent whole-body luminescence images are shown in Figure 3C. Significant accumulations in the spleen and kidneys were observed at early time points, corroborating the results obtained from the PET study. The tumor also had a prominent signal, suggesting the potential use of these ^{64}Cu-doped QDs for Cerenkov luminescence cancer imaging. At 42 h postinjection, the tumor signal was still detectable although it was substantially weakened due to the decay of ^{64}Cu. A 42-h postinjection image of the tumor area is shown in Figure 3D. The photon flux captured via a filter with wavelength of 575 nm was found to be around one-third of the total photon flux captured in the open window ranging from 400 to 920 nm. For free ^{64}Cu, the photon flux of 575 nm was only around 15% of the total flux. The total photon flux detected here comprises two parts: the CL produced by ^{64}Cu (more intense below 500 nm) and the photons emitted by QD580 via CRET (with a peak of 575 nm). The increased signal at 575 nm demonstrates that our ^{64}Cu-doped QDs could efficiently red-shift CL to the emission wavelength of QDs even in living animals during circulation which provides an efficient way to utilize radioactive energy for in vivo applications.

To conclude, we prepared a series of self-illuminating QDs with various emission wavelengths. It is the first time for direct doping of ^{64}Cu PET isotope into QDs via a cation-exchange reaction and endowing them with luminescence properties. It provides a simpler and more rigid "chelator-free" method for radiolabeling, applicable not only to QDs but also to other inorganic nanoparticles. These QDs offer at least two distinct features: (1) favorable imaging without the issue of dissociation of ^{64}Cu from the particles and (2) controllable and enhanced long-wavelength luminescence emission detectable by in vivo imaging. The synergistic advantage of PET and Cerenkov luminescence and the high tumor-targeting ability make these QDs promising agents for multimodal cancer imaging.

■ ASSOCIATED CONTENT

Supporting Information

Experimental and characterization details. This material is available free of charge via the Internet at http://pubs.acs.org.

■ AUTHOR INFORMATION

Corresponding Author

shawn.chen@nih.gov

Author Contributions

[§]X.S. and X.H. contributed equally to this work.

Notes

The authors declare no competing financial interest.

■ ACKNOWLEDGMENTS

This work is supported by the Intramural Research Program (IRP) of the NIBIB, NIH.

■ REFERENCES

(1) Ntziachristos, V.; Ripoll, J.; Wang, L. H. V.; Weissleder, R. *Nat. Biotechnol.* **2005**, *23*, 313.
(2) Wagnieres, G. A.; Star, W. M.; Wilson, B. C. *Photochem. Photobiol.* **1998**, *68*, 603.
(3) Luker, G. D.; Luker, K. E. *J. Nucl. Med.* **2008**, *49*, 1.
(4) Sun, Y.; Zhou, B.; Lin, Y.; Wang, W.; Fernanodo, K. A. S.; Pathak, P.; Meziani, M. J.; Harruff, B. A.; Wang, X.; Wang, H.; Luo, P. G.; Yang, Hua; Kose, M. E.; Chen, B.; Veca, L. M.; Xie, S. *J. Am. Chem. Soc.* **2006**, *128*, 7756.
(5) Baker, S. N.; Baker, G. A. *Angew. Chem., Int. Ed.* **2010**, *49*, 6726.
(6) Wang, F.; Liu, X. *Chem. Soc. Rev.* **2009**, *38*, 976.
(7) Yang, Y.; Shao, Q.; Deng, R.; Wang, C.; Teng, X.; Cheng, K.; Cheng, Z.; Huang, L.; Liu, Z.; Liu, X.; Xing, B. *Angew. Chem., Int. Ed.* **2012**, *51*, 3125.
(8) Michalet, X. E.; Pinaud, F. F.; Bentolila, L. A.; Tsay, J. M.; Doose, S.; Li, J. J.; Sundaresan, G.; Wu, A. M.; Gambhir, S. S.; Weiss, S. *Science* **2005**, *307*, 538.
(9) Yong, K. T. *Theranostics* **2012**, *2*, 629.
(10) Gao, X.; Cui, Y.; Levenson, R. M. *Nat. Biotechnol.* **2004**, *22*, 969.
(11) Pavel, Z.; Mark, S.; Gao, X. *Chem. Soc. Rev.* **2010**, *39*, 4326.
(12) Rizvi, S. B.; Keshtgar, M.; Seifalian, A. M. *Handbook Nanophys.* **2011**, *7*, 1/1−1/11.
(13) Frangioni, J. V. *Curr. Opin. Chem.Biol.* **2003**, *5*, 626.
(14) So, M.; Xu, C.; Loening, A. M.; Gambhir, S. S.; Rao, J. *Nat. Biotechnol.* **2006**, *24*, 339.
(15) Zhang, N.; Francis, K. P.; Prakash, A.; Ansaldi, D. *Nat. Med.* **2013**, *19*, 500.
(16) Thorek, D. L.; Ogirala, A.; Beattie, B. J.; Grimm, J. *Nat. Med.* **2013**, *19*, 1345.
(17) Dragavon, J.; Blazquez, S.; Rekiki, A.; Samson, C.; Theodorou, I.; Rogers, K. L.; Tournebize, R.; Shorte, S. L. *Proc. Natl. Acad. Sci. U.S.A.* **2012**, *109*, 8890.
(18) Robertson, R.; Germanos, M. S.; Li, C.; Mitchell, G. S.; Cherry, S. R.; Silva, M. D. *Phys. Med. Biol.* **2009**, *54*, 355.
(19) Liu, H. G.; Ren, G.; Miao, Z.; Zhang, X. F.; Tang, X. D.; Han, P. Z.; Gambhir, S. S.; Cheng, Z. *PloS One* **2010**, *5*, e9470.
(20) Xu, Y.; Liu, H.; Cheng, Z. *J. Nucl. Med.* **2011**, *52*, 2009.
(21) Liu, H.; Zhang, X.; Xing, B.; Han, P.; Gambhir, S. S.; Cheng, Z. *Small.* **2010**, *6*, 1087.
(22) Kotagiri, N.; Niedzwiedzki, D. M.; Ohara, K.; Achilefu, S. *Angew. Chem., Int. Ed.* **2013**, *52*, 7756.
(23) Bass, L. A.; Wang, M.; Welch, M. J.; Anderson, C. J. *Bioconjugate Chem.* **2000**, *11*, 527.
(24) Schipper, M. L. *Small.* **2009**, *5*, 126.
(25) Son, D. H.; Hughes, S. M.; Yin, Y.; Alivisatos, A. P. *Science* **2004**, *306*, 1009.
(26) Jain, P. K.; Amirav, L.; Aloni, S.; Alivisatos, A. P. *J. Am. Chem. Soc.* **2010**, *132*, 9997.
(27) Luther, J. M.; Zheng, H.; Sadtler, B.; Alivisatos, A. P. *J. Am. Chem. Soc.* **2009**, *131*, 16851.
(28) Thorek, D.; Robertson, R.; Bacchus, W. A.; Hahn, J.; Rothberg, J.; Beattie, B. J.; Grimm, J. *Am. J. Nucl. Med. Mol. Imaging* **2012**, *2*, 163.
(29) Lyer, A. K.; Khaled, G.; Fang, J.; Maeda, H. *Drug Discovery Today* **2006**, *11*, 812.
(30) Cai, W.; Chen, K.; Li, Z.; Gambhir, S. S.; Chen, X. *J. Nucl. Med.* **2007**, *48*, 1862.